analytical chemistry

Article

pubs.acs.org/ac

Probing Spatial Proximity of Supported Lipid Bilayers to Silica Surfaces by Localized Surface Plasmon Resonance Sensing

Abdul Rahim Ferhan,[†] Joshua A. Jackman,[†] and Nam-Joon Cho*[,†,‡]

[†]School of Materials Science and Engineering, Nanyang Technological University, 50 Nanyang Avenue, 639798, Singapore

[‡]School of Chemical and Biomedical Engineering, Nanyang Technological University, 62 Nanyang Drive, 637459, Singapore

Supporting Information

ABSTRACT: On account of high surface sensitivity, localized surface plasmon resonance (LSPR) sensors have proven widely useful for studying lipid membrane configurations at solid−liquid interfaces. Key measurement capabilities include distinguishing adsorbed vesicles from supported lipid bilayers (SLBs) as well as profiling the extent of deformation among adsorbed vesicles. Such capabilities rely on detecting geometrical changes in lipid membrane configuration on a length scale that is comparable to the decay length of the LSPR-induced electromagnetic field enhancement (∼5−20 nm). Herein, we report that LSPR sensors are also capable of probing nanoscale (∼1 nm) variations in the distance between SLBs and underlying silica-coated surfaces. By tuning the electrostatic properties of lipid membranes, we could modulate the bilayer−substrate interaction and corresponding separation distance, as verified by simultaneous LSPR and quartz crystal microbalance-dissipation (QCM-D) measurements. Theoretical calculations of the expected variation in the LSPR measurement response agree well with experimental results and support that the LSPR measurement response is sensitive to subtle variations in the bilayer−substrate separation distance.

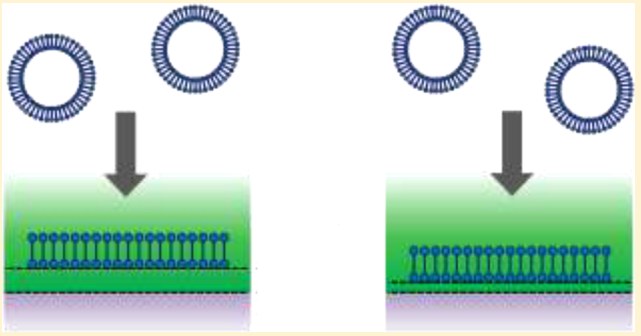

The design of biomimetic assemblies at solid−liquid interfaces offers great potential for a wide range of analytical applications including nanopores,[1] biosensing,[2] and electrophoresis.[3] Achieving precise control over the fabrication of these assemblies and how they are interfaced with supporting surfaces plays an important role in modulating their functionalities.[4−7] In particular, design strategies that rely on molecular self-assembly are desirable, and the spontaneous formation of supported lipid membranes that mimic cellular membranes is a promising example.[8] The structural properties of supported lipid membranes vary greatly depending on the system under consideration, and the need for detailed characterization of their membrane architectures and corresponding lipid−substrate interactions has led to the development of numerous surface-sensitive measurement approaches.[9,10]

One of the most promising approaches involves localized surface plasmon resonance (LSPR) sensors, which have demonstrated excellent merits for investigating supported lipid membranes at solid−liquid interfaces due to their label-free measurement format, simple optical requirements, and high surface sensitivity.[9,11−13] When incident light interacts with metallic nanoparticles on a dielectric support, it causes the collective oscillation of free electrons in the metal's conduction band, which gives rise to LSPR generation and leads to amplification of the electromagnetic field around the nanoparticle's surface.[14,15] The maximum intensity of optical extinction occurs at the plasmon resonance frequency (λ_{max}) and the wavelength position of λ_{max} depends on the local dielectric environment. In particular, the adsorption of biomacromolecules such as phospholipid vesicles typically causes a net positive $\Delta\lambda_{max}$ shift because organic molecules have a higher refractive index than solvent molecules and consequently their adsorption causes a change in the local dielectric environment.[13,16] From a sensing perspective, one of the most advantageous features of LSPR sensors is that the decay length of the electromagnetic field amplification is short and comparable to the height dimension of supported lipid membranes, and hence the sensors are particularly sensitive to the geometrical configuration and conformational properties of adsorbed phospholipid membranes.

A classic example where such discrimination is warranted involves the formation of conformal, ∼5 nm-thick supported lipid bilayers (SLBs) on inorganic surfaces such as silica.[17,18] When lipid vesicles adsorb onto silica surfaces, they typically adsorb intact until reaching a critical surface coverage at which point the adsorbed vesicles begin to rupture and lipids reassemble to form an SLB.[19−22] A key driving force of the SLB formation process is the lipid−substrate interaction, and the interaction strength can influence the kinetic pathway of

Received: January 30, 2017
Accepted: March 15, 2017
Published: March 15, 2017

DOI: 10.1021/acs.analchem.7b00370
Anal. Chem. 2017, 89, 4301−4308

vesicle adsorption and spontaneous rupture, including affecting the intermediate step of vesicle deformation.[21−25] Jonsson et al. demonstrated that nanoplasmonic sensors can detect the onset of vesicle rupture on silica-coated nanohole surfaces because ensuing SLB formation results in the total, adsorbed lipid mass being, on average, closer to the sensor surface and therefore in a region of higher field intensity.[26,27] Similar detection capabilities for tracking the SLB formation process have also been realized using silica-coated gold nanodisk arrays.[4,28] In addition, LSPR sensors can quantitatively profile finer differences in the extent of deformation of adsorbed, intact vesicles as lipids in a more deformed vesicle are, on average, in a region of higher field intensity.[29−32] Another emerging topic of interest concerns location-specific binding of supported lipid membranes, as demonstrated for detection of intact lipid vesicle binding to different regions of nanomenhir structures.[33]

Within this context, there is excellent potential for exploring the utility of LSPR sensors to probe the spatial proximity of SLBs to silica surfaces. Indeed, SLBs are separated from the underlying silica support by a thin hydration layer of interfacial water[34] and it can influence SLB properties such as phase transition behavior.[35] In the literature, the thickness of this hydration layer is often estimated to be around 1−2 nm,[36−38] although direct measurements of its thickness are sparse. Neutron scattering experiments and modeling have estimated that the hydration layer thickness for zwitterionic SLBs on silica surfaces is around 1.5 nm.[39,40] More recently, Zwang et al. utilized a combination of quartz crystal microbalance-dissipation (QCM-D) and dual polarization interferometry (DPI) experiments to calculate that the hydration layer thickness is around 1.0 nm.[41] Of note, the calculations assumed that the density of interfacial water is equivalent to the bulk density of water[42] although the specific density of interfacial water strongly depends on the molecular-level interactions of water molecules and associated ions with silica-based surfaces.[43] While LSPR sensors are largely insensitive to the mass and density properties of interfacial water, the fact that the hydration layer is adjacent to the sensor surface within the region of highest field intensity offers the intriguing possibility that nanometer-scale variations in hydration layer thickness might be resolved based on SLB proximity to the silica-coated surface.

Toward this goal, herein, we have investigated the SLB formation process on silica-coated surfaces by simultaneous LSPR and QCM-D measurements and deciphered the role of membrane surface charge on the formation kinetics and resulting SLB properties. Following this approach, we could modulate the bilayer-substrate interaction and corresponding separation distance, as verified by the LSPR and QCM-D measurement shifts. Theoretical calculations of the expected variation in LSPR measurement response agree well with the experimental results and support that the LSPR measurement response is sensitive to subtle variations in the bilayer−substrate separation distance. Taken together, the findings in this work demonstrate that LSPR sensors are capable of probing nanoscale (∼1 nm) variations in the distance between SLBs and underlying silica-coated surfaces.

MATERIALS AND METHODS

Vesicle Preparation. 1,2-Dioleoyl-*sn*-glycero-3-phosphocholine (PC) and 1-palmitoyl-2-oleoyl-*sn*-glycero-3-ethylphosphocholine (chloride salt) (EPC) lipids were obtained as dispersions in chloroform (Avanti Polar Lipids, Alabaster, AL). Small unilamellar vesicles composed of PC, EPC, or mixtures thereof were prepared by the extrusion method, as previously described.[44] Briefly, the process involves first drying lipids in chloroform with a stream of nitrogen gas to form a dried lipid film. The dried film was rehydrated in aqueous buffer solution (10 mM Tris [pH 7.5] with 150 mM NaCl) at 5 mg/mL lipid concentration, followed by vortexing to aid mixing. Seventeen cycles of mechanical extrusion were performed using track-etched polycarbonate membranes with a diameter of 50 nm. Vesicles were diluted to 0.2 mg/mL concentration in buffer solution before experiment and the stocks were used within 24 h of preparation. All solutions were prepared with Milli-Q-treated water that had a minimum electrical resistivity of 18.2 MΩ cm (Millipore, Billerica, MA).

Dynamic Light Scattering. Dynamic light scattering (DLS) measurements were conducted using a 90Plus Particle Size Analyzer instrument (Brookhaven Instruments Corporation, Holtsville, NY). The DLS measurements were taken at a scattering angle of 90° because the reflection effect is minimized at this condition. The results were analyzed using the method of cumulants to obtain the intensity-weighted vesicle size distribution, including the average effective vesicle diameter (z-average diameter) and polydispersity. The z-average diameter obtained for all extruded vesicle samples was below 60 nm and the polydispersity index was below 0.1.

Combined Measurement Setup. The combined QCM-D and LSPR setup is based on a Q-Sense E1 instrument that is fitted with the Q-Sense QWM401 window module (Biolin Scientific AB, Stockholm, Sweden) and the Insplorion Acoulyte module (Insplorion AB, Gothenburg, Sweden). The Acoulyte module provides an optical connection between the measurement chamber and the Insplorion X-Nano optics unit (Insplorion AB). Detailed description of the measurement setup can be found in refs 45 and 46. Measurements were performed on modified quartz crystal sensors, the surface of which consists of randomly distributed, silica-coated gold nanodisks prepared by hole-mask colloidal lithography[47] followed by sputtering. The gold nanodisks had an average height and diameter of ∼20 and ∼100 nm, respectively, and were covered with a thin layer of silica (thickness ∼10 nm). The bulk sensitivity of the coated nanodisks was approximately 114 nm per refractive index unit (RIU), as determined by solvent-exchange experiments with water/glycerol mixtures of varying RI. Before the experiment, the sensor chip was soaked in a 1% v/v sodium dodecyl sulfate (SDS) solution for 30 min and then sequentially rinsed with water and ethanol. A stream of nitrogen gas was used to dry the sensor chip, which was then treated with oxygen plasma for 30 s.

Data Analysis. LSPR data analysis was conducted using the Insplorer software package (Insplorion AB). The centroid position of the LSPR peak in the extinction spectrum was evaluated by high-order polynomial fitting as previously described,[48] and is denoted as the LSPR peak position in this work. QCM-D data analysis was conducted by using the Voigt-Voinova model[49] that is available in the Q-Tools software package (Biolin Scientific AB). More detailed information can be found in the Supporting Information.

RESULTS AND DISCUSSION

Measurement Strategy. Simultaneous LSPR and QCM-D measurements were conducted in order to characterize the SLB formation process and resulting SLB properties. The sensor substrate consisted of a quartz crystal sensor chip upon which a

DOI: 10.1021/acs.analchem.7b00370
Anal. Chem. 2017, 89, 4301−4308

random arrangement of noninteracting, silica-coated gold nanodisks was fabricated, as described in the Materials and Methods section. As reported in recent works,[45,46] the two label-free experimental techniques are highly complementary with respect to measurement principle and probing volume. By combining the two measurement techniques that rely on different physical principles, there is excellent potential for gaining insight into detailed biomacromolecular features such as surface hydration that are difficult to unravel by either technique alone. Indeed, while extensive efforts have been placed at pairing label-free acoustic and optical sensor techniques as well as other related techniques (e.g., electrochemistry[50]), one distinct advantage of simultaneous measurements with QCM-D and LSPR is that the probing volume of LSPR is particularly small compared to other optical sensor possibilities such as ellipsometry[51] and reflectometry.[52] The resulting high surface sensitivity makes LSPR an attractive candidate for characterizing biomimetic assemblies that are in close contact with sensor surfaces. Furthermore, in the present case, the QCM-D measurement responses provide verification for the LSPR sensor response and aid data analysis.

LSPR is an optical sensor technique that is sensitive to changes in local refractive index near the sensor surface and hence the decay length of the evanescent electromagnetic field is around 5−20 nm,[28,53,54] which is within the range of an SLB coating on the sensor surface (Figure 1A). As a result, LSPR detection is sensitive to both the surface coverage and spatial proximity of the biomacromolecular adsorbate as organic molecules such as phospholipids typically have a higher refractive index than aqueous buffer solution, but the LSPR measurement is not sensitive to solvent that is coupled to the adsorbed biomacromolecules because the solvent molecules have the same refractive index as the bulk solution. When biomacromolecules, lipid vesicles in the present case adsorb, and rupture to form an SLB on the sensor surface, there is a change in the local refractive index and a resulting shift in the resonance wavelength, $\Delta\lambda_{max}$, at which maximum light extinction occurs. In the current experiments, different fluid-phase lipid compositions were utilized based on mixtures of zwitterionic 1,2-dioleoyl-*sn*-glycero-3-phosphocholine (PC) lipid and cationic 1-palmitoyl-2-oleoyl-*sn*-glycero-3-ethylphosphocholine (EPC) lipid. The selected compositions of increasing positive surface charge were 100 mol % PC, 50 mol % PC/50 mol % EPC, and 100 mol % EPC. In accordance with the LSPR measurement principle, vesicle adsorption and rupture on the sensor surface led to a positive $\Delta\lambda_{max}$ shift based on the spectral signature (Figure 1B). To gain further insight into the SLB formation process, $\Delta\lambda_{max}$ was tracked as a function of time in order to characterize the process of vesicle adsorption and spontaneous rupture along with the final SLB properties. By taking into account the known refractive index of an SLB on silica, it was also possible to estimate the bound, optical mass based on the $\Delta\lambda_{max}$ shift, which reflects the mass contribution from adsorbed phospholipid molecules but not coupled solvent.

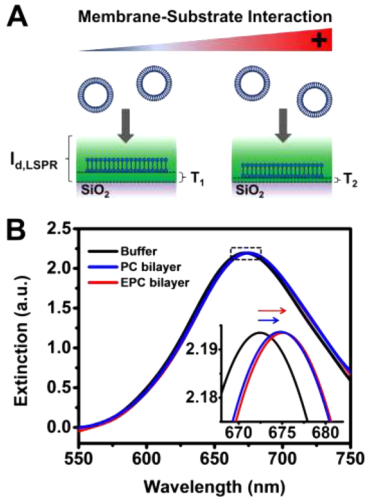

Figure 1. Measurement principle of LSPR proximity sensing. (A) Schematic illustration of SLB membranes on a silica-coated substrate at different distances from the sensor surface. The decay length (l_d) of the LSPR-induced electromagnetic field enhancement is presented for comparison, and T denotes the hydration layer thickness. The adsorption kinetics of SLB formation and resulting spatial proximity of SLBs to the sensor surface were controlled by adjusting the strength of the membrane−substrate interaction with respect to membrane surface charge. (B) Optical extinction spectra from the LSPR measurements show that the λ_{max} position shifts after SLB formation from zwitterionic PC and positively charged EPC membrane compositions. Inset shows an enlargement of the area bound by the dashed rectangle.

On the other hand, QCM-D is an acoustic sensor technique that is sensitive to both adsorbed macromolecules and hydrodynamic-coupled solvent molecules and therefore can distinguish adsorbed phospholipids in different configurations (e.g., intact vesicle versus SLB).[55] QCM-D measurements track changes in the resonance frequency and energy dissipation of the sensor chip in order to probe the mass and viscoelastic properties of the adsorbate, respectively.[56] Importantly, QCM-D is a well-validated measurement approach for studying lipid vesicle adsorption and therefore offers a reference tool to verify SLB formation in parallel to the LSPR measurements. Furthermore, in complement to the particularly high surface sensitivity of the LSPR technique, the QCM-D technique has a longer penetration depth of around 60−250 nm. In cases of low-energy dissipation, the Sauerbrey model can be applied to calculate the amount of bound, acoustic mass based on a linear relationship between the frequency shift and mass.[57] In cases of high energy dissipation, more sophisticated models such as the Voigt−Voinova model can be applied in order to determine the acoustic mass by taking into account the viscoelastic contribution.[58] It should be emphasized that the optical mass determined by the LSPR measurement technique reflects only bound phospholipid molecules, whereas the acoustic mass determined by the QCM-D measurement technique is sensitive to both phospholipid and hydrodynamically coupled solvent molecules. Hence, the combination of LSPR and QCM-D measurements can also determine the hydration mass of sufficiently thin films (e.g., SLBs) on the sensor surface.

SLB Formation Process. On the basis of this measurement approach, the interaction between lipid vesicles and the silica-coated surface was investigated as a function of varying membrane surface charge. Indeed, as the electrostatic interaction between vesicles and the silica surface becomes increasingly attractive, different adsorption pathways are possible to obtain,[22,23,59] and it is anticipated that the varying bilayer−substrate interaction strength would also influence the corresponding separation distance. In Figure 2, the QCM-D and LSPR adsorption kinetics for vesicle adsorption and rupture leading to SLB formation are presented for all three lipid compositions. The QCM-D frequency shift response

DOI: 10.1021/acs.analchem.7b00370
Anal. Chem. 2017, 89, 4301−4308

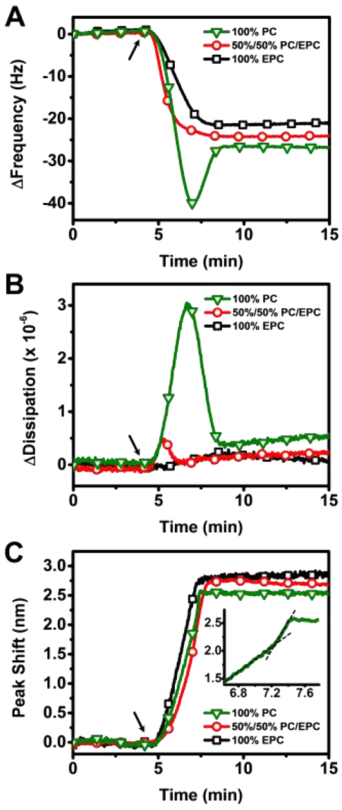

Figure 2. Effect of membrane surface charge on SLB formation kinetics. QCM-D (A) frequency and (B) dissipation shifts and (C) LSPR peak shifts are recorded as a function of time. The inset in panel C shows the characteristic kink in the LSPR response, which is associated with the onset of vesicle rupture at a critical surface coverage of adsorbed vesicles. Baseline signals were obtained in aqueous buffer solution before vesicles were added in equivalent buffer solution under continuous flow conditions from around t = 5 min (see arrow).

showed that 100% PC vesicles adsorbed until reaching a critical surface coverage around −40 Hz, followed by vesicle rupture and SLB formation with a final frequency shift value around −27 Hz, which agrees well with expected values (Figure 2A). By contrast, EPC-containing vesicles appeared to rupture without requiring a critical coverage and the QCM-D frequency shifts showed one-step kinetics yielding final frequency shifts of −21 and −24 Hz for 100% EPC and 50%/50% PC/EPC lipid compositions, respectively. Hence, with increasing positive surface charge, there was a marked transition from two-step to one-step SLB formation kinetics as well as smaller final frequency shifts. The corresponding QCM-D energy dissipation shifts are consistent with these findings as there was a maximum in the energy dissipation shift around 3×10^{-6} for 100% PC vesicles that corresponds to the critical coverage (Figure 2B). By contrast, there was essentially no change in the energy dissipation shifts for the 100% EPC and 50%/50% PC/EPC lipid compositions. In all cases, the final energy dissipation shift was less than 0.5×10^{-6}, which is consistent with SLB formation.

In parallel measurements, the LSPR signal showed a monotonic increase in peak shift up to saturation for all cases (Figure 2C). Upon closer inspection, a characteristic kink in the LSPR signal originating from vesicle rupture upon reaching a critical coverage was clearly observed for the 100% PC lipid composition, while there was no kink for the 100% EPC and 50%/50% PC/EPC lipid compositions. This trend agrees well with the QCM-D measurements and supports that the PC lipid vesicles rupture to form SLBs via a two-step pathway whereas the EPC-containing lipid vesicles form SLBs via a one-step pathway. Interestingly, the final values of the LSPR peak shift were higher with increasing positive surface charge of the lipid composition. The final peak shift for the 100% PC SLB was 2.5 nm, and the final peak shifts were 2.7 and 2.8 nm for 50%/50% PC/EPC and 100% EPC SLBs, respectively. Importantly, while the final $\Delta\lambda_{max}$ values for PC and EPC SLBs varied by only around 0.3 nm, this range is more than 30-times larger than the sensor resolution, which is defined as the smallest change in the bulk refractive index that produced a detectable change in the sensor output.[60] For these experiments, the resolution was determined to be around 6.27×10^{-5} RIU, which corresponds to a peak shift of around 0.007 nm (details are provided in the Supporting Information).

Considering that the phospholipids have similar optical properties in all cases,[61] the observed trend indicates that more positively charged SLBs are closer to the sensor surface (smaller separation distance), which is reasonable considering that the silica surface is negatively charged under the experimental conditions.[38] Furthermore, the LSPR-measured trend in SLB peak shift values is opposite to the trend observed for the final values of the QCM-D frequency shifts, highlighting the different measurement principles of the two techniques. The LSPR measurement is sensitive only to the spatial proximity of phospholipid molecules in the SLB with respect to the sensor surface, with increased measurement shifts occurring for SLBs nearer to the sensor surface. On the other hand, the QCM-D measurement is sensitive to the phospholipid molecules in the SLB along with hydrodynamically coupled solvent molecules between the SLB and underlying solid support (the so-called hydration layer). When the SLB is nearer to the sensor surface, the hydration layer is thinner and hence the QCM-D frequency shift is smaller, as seen in our experiments for SLBs with increasingly positive surface charge. Hence, the LSPR and QCM-D experiments show excellent agreement to verify SLB formation and demonstrate that positively charge SLBs are nearer to the silica-coated sensor surface and possess thinner hydration layers.

Vesicle-to-Bilayer Structural Transformation. In order to further scrutinize the vesicle-to-bilayer structural transformation, we first plotted the time-independent frequency–dissipation (f–D) curves (Figure 3A). For the 100% PC case, the f–D curves displayed a characteristic cusp, with an inflection point that signifies vesicle rupture after reaching a critical coverage. In marked contrast, the 100% EPC case showed an f–D curve that forms a nearly flat, horizontal line that is consistent with immediate rupture of adsorbing vesicles. In between these two cases lies the intermediate 50%/50% PC/EPC case for which there was an initially positive slope that returned downward upon reaching a frequency shift around −10 Hz onward. Compared to the 100% PC case, the 50%/50% PC/EPC case also exhibited a shallower initial positive slope, indicating that adsorbed 50%/50% PC/EPC lipid vesicles are more deformed than 100% PC lipid vesicles.[62]

In addition, the corresponding time-independent peak shift–frequency (λ–f) curves were also plotted (Figure 3B). For the 100% PC case, three stages were observed relating to intact vesicle adsorption, vesicle rupture, and release of coupled solvent. Interestingly, the 100% EPC case showed a nearly

DOI: 10.1021/acs.analchem.7b00370
Anal. Chem. 2017, 89, 4301−4308

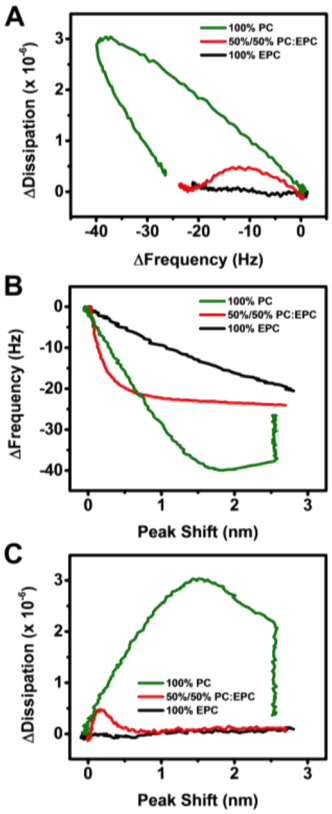

Figure 3. Analysis of vesicle-to-bilayer structural transformation. (A) Time-independent plot of QCM-D frequency versus energy dissipation shifts ($f-D$ curves). (B) Time-independent plot of QCM-D frequency shifts versus LSPR peak shifts ($\lambda-f$ curves). (C) Time-independent plot of QCM-D energy dissipation shifts versus LSPR peak shifts ($\lambda-D$ curves).

linear increase in frequency shift and peak shift in one stage, which is consistent with the immediate rupture of adsorbing vesicles. On the other hand, the 50%/50% PC/EPC case again showed intermediate behavior as two stages were observed indicating initial vesicle adsorption followed by nearly immediate rupture of adsorbing vesicles at higher surface coverages.

The time-independent peak shift−dissipation ($\lambda-D$) curves further support the general trends observed with the different lipid compositions (Figure 3C). Similar to the $\lambda-f$ curves, the 100% PC case showed a three-stage process relating to intact vesicle adsorption, vesicle rupture, and release of coupled solvent. The slope of the 100% EPC case was also nearly negligible, further supporting that the adsorbed vesicles rupture immediately upon contact with the silica surface. In this case, the 50%/50% PC/EPC case exhibited nearly identical behavior to the 100% PC case except for a smaller initial increase and drop at low surface coverage. Hence, with increasing positive surface charge, SLB formation transitions from a two-step to one-step process on account of more attractive vesicle−substrate interactions. This finding is in excellent agreement with a previous report[22] that utilized a combination of QCM-D and atomic force microscopy experiments to identify that zwitterionic vesicles adsorb onto silica surfaces until reaching a critical coverage before collectively rupturing to form an SLB whereas positively charged vesicles individually rupture upon adsorption onto silica surfaces to form an SLB.

Quantitative Evaluation of Hydration Mass. In Figure 4, the optical and acoustic mass signatures are presented as a

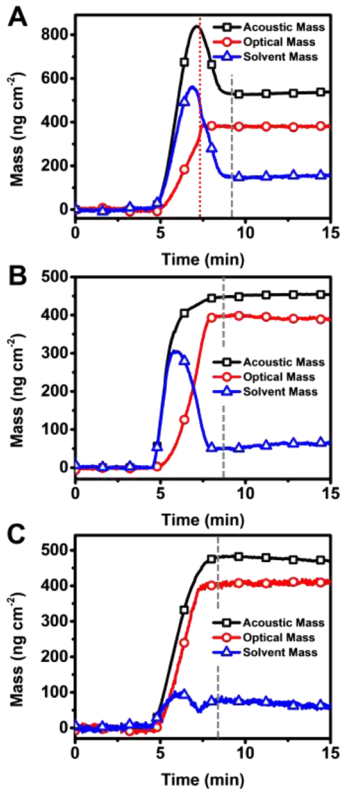

Figure 4. Comparison of hydration mass signatures for SLBs on silica surfaces, which are composed of (A) 100% PC, (B) 50%/50% PC/EPC, or (C) 100% EPC lipid (increasing positive surface charge). The dotted lines serve as a guide to indicate the times when the acoustic (gray line) and optical (red line) masses begin to saturate; for panels B and C, the saturation times for the two masses coincide, and the time point is indicated by the gray line only.

function of time throughout the vesicle-to-bilayer structural transformation along with the hydration (solvent) mass that is calculated from the difference of the optical and acoustic mass values at each time point. For the 100% PC case, the critical coverage yielded acoustic and hydration masses around 840 and 560 ng/cm^2, respectively, while there was a monotonic increase in the optical mass throughout the SLB formation process (Figure 4A). The final acoustic, optical, and hydration masses were 540, 380, and 160 ng/cm^2, respectively. On the other hand, the 50%/50% PC/EPC case showed unique behavior because only the hydration mass signature indicated a critical coverage around 300 ng/cm^2 (Figure 4B). By contrast, the acoustic and optical masses showed monotonic increases. The final acoustic, optical, and hydration masses were 455, 390, and 65 ng/cm^2, respectively. Lastly, no critical coverage was observed in the 100% EPC case and the final acoustic, optical, and hydration masses were 470, 410, and 60 ng/cm^2, respectively (Figure 4C). Hence, with increasing positive surface charge, there was a decreasing amount of hydration mass associated with the SLB, implying that the hydration layer becomes thinner with stronger lipid−substrate interactions.

From an LSPR sensing perspective, one of the most striking implications of this finding is that the LSPR peak shifts appear to be sensitive to the spatial proximity of the SLB to the sensor surface. Indeed, the evanescent electromagnetic field of the

DOI: 10.1021/acs.analchem.7b00370
Anal. Chem. 2017, 89, 4301−4308

plasmon resonance has a maximum field intensity at the sensor surface and the intensity decays with increasing distance from the sensor surface. Typically, the distribution of the field intensity as a function of the distance from the sensor surface is approximated by an exponential decay model with a characteristic decay length L. The effective refractive index, n_{eff}, of the probing volume is denoted by[28,63]

$$n_{eff} = \frac{1}{L}\int_{z=0}^{\infty} n(z)\exp(-z/L)\,dz \quad (1)$$

where $n(z)$ is the refractive index at a distance z above the sensor surface. In our case, $n(z) = n_{buffer}$ for $0 < z < d$, $n(z) = n_{SLB}$ for $d < z < d + T$, and $n(z) = n_{buffer}$ for $d + T < z <$ infinity, where d is the distance from the SLB's lower leaflet to the sensor surface and T is the bilayer thickness. The corresponding LSPR peak shift, $\Delta\lambda_{max}$, that is induced by a change in the local refractive index is given by

$$\Delta\lambda_{max} = S(n_{eff} - n_{buffer}) \quad (2)$$

where S is the bulk sensitivity of the sensor (114 nm/RIU in the present case) and n_{eff} is the refractive index of the buffer solution.

Based on the QCM-D measurement results and Voigt–Voinova model analysis, it was estimated that the total SLB thickness decreased from 6.91 nm for 100% PC to 5.58 nm for 100% EPC, a net difference of 1.33 nm that is assumed to correspond to the difference in the hydration layer thickness. By plotting the total thickness of the SLB film against the hydration fraction, we estimated the dry thickness of the SLB to be around 4.91 nm. Substituting n_{eff} in eq 2 with the integral of eq 1 (with T = 4.91 nm) and correlating it with the LSPR peak shift data for the 100% PC and EPC cases, we estimated that the variation in distance from the sensor surface for the two SLBs is 1.79 nm, which agrees reasonably well with the experimental results. The agreement between experiment and theory reinforces that the LSPR measurement technique is capable of detecting subtle variations in the spatial proximity of SLBs to the sensor surface.

While there have been previous reports that describe how LSPR sensors are able to distinguish between adsorbed, intact vesicles, and SLBs or the extent of deformation of adsorbed vesicles on account of geometrical changes in the lipid membrane configuration,[30,31,64,65] this is the first demonstration of how nanoscale variations in the distance between an SLB with fixed geometry and the sensor surface can be detected based on distance-dependent LSPR measurement responses. In the context of supported lipid membrane systems, such measurement capabilities could also shed light on how the hydration layer influences vesicle adsorption onto titanium oxide surfaces,[66] including the subsequent properties of SLBs prepared via alternative fabrication strategies[67,68] in cases where adsorbed vesicles do not rupture spontaneously. Furthermore, it should be noted that, in this demonstration, the LSPR measurements responses were used to interpret the variation in spatial proximity of the SLB to the sensor surface on a relative scale. The absolute distance from the SLB to the sensor surface is unknown, and the difference in distance for SLBs that have varying degrees of attractive interaction with the silica surface was determined. Given the high sensor resolution as discussed above, it might be formally possible to determine the relative spatial proximity of SLBs to the silica surface in even more subtle cases. However, at a practical level, our measurements are likely at the upper bound of sensitivity for analyzing supported lipid membranes and other biomimetic nanostructures that rely on molecular self-assembly because the variation in LSPR peak shift response for SLB formation in a particular system is typically around ±0.05 nm. These points highlight the fact that SLB platforms offer a two-dimensional biomimetic nanostructure with a planar geometry, allowing us to interpret the LSPR measurement data by utilizing models that are applicable to uniform thin films. This consideration is important because the SLB offers a well-controlled model system to quantitatively investigate these measurement capabilities. Extending such capabilities to analyze the spatial proximity of particle adsorbates will likely require more complex models and might be compatible with other nanoplasmonic sensing formats as well. In the present system, the LSPR measurements were conducted in reflection mode as ensemble-averaged readouts, and other formats such as dark field microscopy on individual nanoparticle transducers[69] might also be possible. Looking forward, there is excellent potential for exploring these demonstrated measurement capabilities of LSPR sensors across various applications in the biointerfacial sciences and beyond.

CONCLUSION

In this work, we have demonstrated that LSPR sensors are capable of probing nanoscale (∼1 nm) variations in the distance between SLBs and underlying silica-coated surfaces. This demonstration was experimentally achieved by tuning the electrostatic properties of lipid membranes in order to modulate the bilayer–substrate interaction and corresponding separation distance. Simultaneous LSPR and QCM-D measurements were conducted in order to determine that vesicle adsorption and spontaneous rupture transitions from a two-step to one-step process with increasingly positive membrane surface charge. In terms of both adsorption kinetics and final SLB properties, it was evident that lipid membranes with more positive surface charge demonstrated more attractive interactions with the negatively charged silica substrate, which manifested itself in quicker SLB formation kinetics as well as tighter coupling to the silica substrate that led to a smaller bilayer–substrate separation distance. As a result, there was a smaller hydration mass in the resulting SLB with increasing positive membrane surface charge. Owing to the different measurement sensitivities of the two measurement techniques, stronger bilayer–substrate interactions and correspondingly smaller hydration layer thicknesses increased the LSPR measurement response while the QCM-D measurement response decreased. Theoretical calculations of the expected variation in LSPR measurement response agree well with the experimental results based on distance-dependent variations in the evanescent electromagnetic field intensity and support that the LSPR measurement response is sensitive to subtle variations in the bilayer–substrate separation distance. Looking forward, such capabilities extend the scope of LSPR measurements beyond detecting conformational changes in biomacromolecules, such as proteins and lipid vesicles, and highlight the high surface sensitivity to probe the spatial proximity of biomacromolecules near sensor surfaces.

ASSOCIATED CONTENT

Supporting Information

The Supporting Information is available free of charge on the ACS Publications website at DOI: 10.1021/acs.analchem.7b00370.

DOI: 10.1021/acs.analchem.7b00370
Anal. Chem. 2017, 89, 4301–4308

Experimental methods and LSPR data analysis (PDF)

AUTHOR INFORMATION

Corresponding Author

*E-mail: njcho@ntu.edu.sg.

ORCID

Nam-Joon Cho: 0000-0002-8692-8955

Notes

The authors declare no competing financial interest.

ACKNOWLEDGMENTS

This work was supported by a National Research Foundation Proof-of-Concept Grant (Grant NRF2015NRF-POC001-019).

REFERENCES

(1) Yusko, E. C.; Johnson, J. M.; Majd, S.; Prangkio, P.; Rollings, R. C.; Li, J.; Yang, J.; Mayer, M. *Nat. Nanotechnol.* **2011**, *6*, 253−260.
(2) Bally, M.; Bailey, K.; Sugihara, K.; Grieshaber, D.; Vörös, J.; Städler, B. *Small* **2010**, *6*, 2481−2497.
(3) Liu, C.; Monson, C. F.; Yang, T.; Pace, H.; Cremer, P. S. *Anal. Chem.* **2011**, *83*, 7876−7880.
(4) Zan, G. H.; Jackman, J. A.; Kim, S. O.; Cho, N. J. *Small* **2014**, *10*, 4828−4832.
(5) Tatsuno, T.; Okamoto, T.; Ezaki, T.; Isobe, T.; Nakajima, A.; Matsushita, S. *Bull. Chem. Soc. Jpn.* **2016**, *89*, 369−374.
(6) Ariga, K. *Anal. Sci.* **2016**, *32*, 1141−1149.
(7) Jackman, J. A.; Linardy, E.; Yoo, D.; Seo, J.; Ng, W. B.; Klemme, D. J.; Wittenberg, N. J.; Oh, S.-H.; Cho, N.-J. *Small* **2016**, *12*, 1159−1166.
(8) Ariga, K. *ChemNanoMat* **2016**, *2*, 333−343.
(9) Mashaghi, A.; Mashaghi, S.; Reviakine, I.; Heeren, R. M.; Sandoghdar, V.; Bonn, M. *Chem. Soc. Rev.* **2014**, *43*, 887−900.
(10) Wang, D.-S.; Fan, S.-K. *Sensors* **2016**, *16*, 1175.
(11) Galush, W. J.; Shelby, S. A.; Mulvihill, M. J.; Tao, A.; Yang, P.; Groves, J. T. *Nano Lett.* **2009**, *9*, 2077−2082.
(12) Mayer, K. M.; Hafner, J. H. *Chem. Rev.* **2011**, *111*, 3828−3857.
(13) Dahlin, A. B.; Wittenberg, N. J.; Höök, F.; Oh, S.-H. *Nanophotonics* **2013**, *2*, 83−101.
(14) Willets, K. A.; Van Duyne, R. P. *Annu. Rev. Phys. Chem.* **2007**, *58*, 267−297.
(15) Anker, J. N.; Hall, W. P.; Lyandres, O.; Shah, N. C.; Zhao, J.; Van Duyne, R. P. *Nat. Mater.* **2008**, *7*, 442−453.
(16) Estevez, M.-C.; Otte, M. A.; Sepulveda, B.; Lechuga, L. M. *Anal. Chim. Acta* **2014**, *806*, 55−73.
(17) Boxer, S. G. *Curr. Opin. Chem. Biol.* **2000**, *4*, 704−709.
(18) Castellana, E. T.; Cremer, P. S. *Surf. Sci. Rep.* **2006**, *61*, 429−444.
(19) McConnell, H. M.; Watts, T. H.; Weis, R. M.; Brian, A. A. *Biochim. Biophys. Acta, Rev. Biomembr.* **1986**, *864*, 95−106.
(20) Watts, T. H.; Brian, A. A.; Kappler, J. W.; Marrack, P.; McConnell, H. M. *Proc. Natl. Acad. Sci. U. S. A.* **1984**, *81*, 7564−7568.
(21) Richter, R. P.; Bérat, R.; Brisson, A. R. *Langmuir* **2006**, *22*, 3497−3505.
(22) Richter, R.; Mukhopadhyay, A.; Brisson, A. *Biophys. J.* **2003**, *85*, 3035−3047.
(23) Reimhult, E.; Höök, F.; Kasemo, B. *Langmuir* **2003**, *19*, 1681−1691.
(24) Cha, T.; Guo, A.; Zhu, X. Y. *Biophys. J.* **2006**, *90*, 1270−1274.
(25) Jackman, J. A.; Tabaei, S. R.; Zhao, Z.; Yorulmaz, S.; Cho, N.-J. *ACS Appl. Mater. Interfaces* **2015**, *7*, 959−968.
(26) Jonsson, M. P.; Jönsson, P.; Dahlin, A. B.; Höök, F. *Nano Lett.* **2007**, *7*, 3462−3468.
(27) Jonsson, M. P.; Jönsson, P.; Höök, F. *Anal. Chem.* **2008**, *80*, 7988−7995.
(28) Larsson, E. M.; Edvardsson, M. E. M.; Langhammer, C.; Zorić, I.; Kasemo, B. *Rev. Sci. Instrum.* **2009**, *80*, 125105.
(29) Jackman, J. A.; Zhdanov, V. P.; Cho, N.-J. *Langmuir* **2014**, *30*, 9494−9503.
(30) Oh, E.; Jackman, J. A.; Yorulmaz, S.; Zhdanov, V. P.; Lee, H.; Cho, N.-J. *Langmuir* **2015**, *31*, 771−781.
(31) Dacic, M.; Jackman, J. A.; Yorulmaz, S.; Zhdanov, V. P.; Kasemo, B.; Cho, N.-J. *Langmuir* **2016**, *32*, 6486−6495.
(32) Jackman, J. A.; Yorulmaz Avsar, S.; Ferhan, A. R.; Li, D.; Park, J. H.; Zhdanov, V. P.; Cho, N.-J. *Anal. Chem.* **2017**, *89*, 1102−1109.
(33) Kumar, K.; Dahlin, A. B.; Sannomiya, T.; Kaufmann, S.; Isa, L.; Reimhult, E. *Nano Lett.* **2013**, *13*, 6122−6129.
(34) Sackmann, E. *Science* **1996**, *271*, 43.
(35) Seeger, H. M.; Cerbo, A. D.; Alessandrini, A.; Facci, P. *J. Phys. Chem. B* **2010**, *114*, 8926−8933.
(36) Cremer, P. S.; Boxer, S. G. *J. Phys. Chem. B* **1999**, *103*, 2554−2559.
(37) Wiegand, G.; Arribas-Layton, N.; Hillebrandt, H.; Sackmann, E.; Wagner, P. *J. Phys. Chem. B* **2002**, *106*, 4245−4254.
(38) Anderson, T. H.; Min, Y.; Weirich, K. L.; Zeng, H.; Fygenson, D.; Israelachvili, J. N. *Langmuir* **2009**, *25*, 6997−7005.
(39) Koenig, B. W.; Krueger, S.; Orts, W. J.; Majkrzak, C. F.; Berk, N. F.; Silverton, J. V.; Gawrisch, K. *Langmuir* **1996**, *12*, 1343−1350.
(40) Doshi, D. A.; Dattelbaum, A. M.; Watkins, E. B.; Brinker, C. J.; Swanson, B. I.; Shreve, A. P.; Parikh, A. N.; Majewski, J. *Langmuir* **2005**, *21*, 2865−2870.
(41) Zwang, T. J.; Fletcher, W. R.; Lane, T. J.; Johal, M. S. *Langmuir* **2010**, *26*, 4598−4601.
(42) Mashaghi, A.; Swann, M.; Popplewell, J.; Textor, M.; Reimhult, E. *Anal. Chem.* **2008**, *80*, 3666−3676.
(43) Kim, J.; Kim, G.; Cremer, P. S. *Langmuir* **2001**, *17*, 7255−7260.
(44) MacDonald, R. C.; MacDonald, R. I.; Menco, B. P. M.; Takeshita, K.; Subbarao, N. K.; Hu, L.-r. *Biochim. Biophys. Acta, Biomembr.* **1991**, *1061*, 297−303.
(45) Ferhan, A. R.; Jackman, J. A.; Cho, N.-J. *Anal. Chem.* **2016**, *88*, 12524−12531.
(46) Ferhan, A. R.; Jackman, J. A.; Cho, N.-J. *Phys. Chem. Chem. Phys.* **2017**, *19*, 2131−2139.
(47) Fredriksson, H.; Alaverdyan, Y.; Dmitriev, A.; Langhammer, C.; Sutherland, D. S.; Zäch, M.; Kasemo, B. *Adv. Mater.* **2007**, *19*, 4297−4302.
(48) Dahlin, A. B.; Tegenfeldt, J. O.; Höök, F. *Anal. Chem.* **2006**, *78*, 4416−4423.
(49) Cho, N.-J.; Kanazawa, K. K.; Glenn, J. S.; Frank, C. W. *Anal. Chem.* **2007**, *79*, 7027−7035.
(50) Briand, E.; Zäch, M.; Svedhem, S.; Kasemo, B.; Petronis, S. *Analyst* **2010**, *135*, 343−350.
(51) Jackman, J. A.; Goh, H. Z.; Zhdanov, V. P.; Knoll, W.; Cho, N.-J. *J. Am. Chem. Soc.* **2016**, *138*, 1406−1413.
(52) Edvardsson, M.; Svedhem, S.; Wang, G.; Richter, R.; Rodahl, M.; Kasemo, B. *Anal. Chem.* **2009**, *81*, 349−361.
(53) Haes, A. J.; Zou, S.; Schatz, G. C.; Van Duyne, R. P. *J. Phys. Chem. B* **2004**, *108*, 109−116.
(54) Whitney, A. V.; Elam, J. W.; Zou, S.; Zinovev, A. V.; Stair, P. C.; Schatz, G. C.; Van Duyne, R. P. *J. Phys. Chem. B* **2005**, *109*, 20522−20528.
(55) Keller, C.; Kasemo, B. *Biophys. J.* **1998**, *75*, 1397−1402.
(56) Cho, N.-J.; Frank, C. W.; Kasemo, B.; Höök, F. *Nat. Protoc.* **2010**, *5*, 1096−1106.
(57) Ferreira, G. N.; Da-Silva, A.-C.; Tomé, B. *Trends Biotechnol.* **2009**, *27*, 689−697.
(58) Voinova, M.; Jonson, M.; Kasemo, B. *Biosens. Bioelectron.* **2002**, *17*, 835−841.
(59) Richter, R. P.; Brisson, A. R. *Biophys. J.* **2005**, *88*, 3422−3433.
(60) Homola, J. *Chem. Rev.* **2008**, *108*, 462−493.
(61) MacDonald, R. C.; Rakhmanova, V. A.; Choi, K. L.; Rosenzweig, H. S.; Lahiri, M. K. *J. Pharm. Sci.* **1999**, *88*, 896−904.
(62) Keller, C.; Glasmästar, K.; Zhdanov, V.; Kasemo, B. *Phys. Rev. Lett.* **2000**, *84*, 5443.
(63) Jung, L. S.; Campbell, C. T.; Chinowsky, T. M.; Mar, M. N.; Yee, S. S. *Langmuir* **1998**, *14*, 5636−5648.

DOI: 10.1021/acs.analchem.7b00370
Anal. Chem. 2017, 89, 4301−4308

(64) Tabaei, S. R.; Choi, J.-H.; Haw Zan, G.; Zhdanov, V. P.; Cho, N.-J. *Langmuir* **2014**, *30*, 10363−10373.
(65) Jackman, J. A.; Spackova, B.; Linardy, E.; Kim, M. C.; Yoon, B. K.; Homola, J.; Cho, N.-J. *Chem. Commun.* **2016**, *52*, 76−79.
(66) Jackman, J. A.; Zan, G. H.; Zhao, Z.; Cho, N.-J. *Langmuir* **2014**, *30*, 5368−5372.
(67) Zan, G. H.; Jackman, J. A.; Cho, N.-J. *J. Phys. Chem. B* **2014**, *118*, 3616−3621.
(68) Tabaei, S. R.; Jackman, J. A.; Kim, S.-O.; Zhdanov, V. P.; Cho, N.-J. *Langmuir* **2015**, *31*, 3125−3134.
(69) Li, T.; Wu, X.; Liu, F.; Li, N. *Analyst* **2017**, *142*, 248−256.

DOI: 10.1021/acs.analchem.7b00370
Anal. Chem. 2017, 89, 4301−4308